



HAL
open science

A record of eruption and intrusion at a fast spreading ridge axis: Axial summit trough of the East Pacific Rise at 9-10°N

S. Adam Adam Soule, Javier Escartin, Daniel J Fornari

► **To cite this version:**

S. Adam Adam Soule, Javier Escartin, Daniel J Fornari. A record of eruption and intrusion at a fast spreading ridge axis: Axial summit trough of the East Pacific Rise at 9-10°N. *Geochemistry, Geophysics, Geosystems*, 2009, 10 (10), 10.1029/2008gc002354 . insu-01875683

HAL Id: insu-01875683

<https://insu.hal.science/insu-01875683>

Submitted on 17 Sep 2018

HAL is a multi-disciplinary open access archive for the deposit and dissemination of scientific research documents, whether they are published or not. The documents may come from teaching and research institutions in France or abroad, or from public or private research centers.

L'archive ouverte pluridisciplinaire **HAL**, est destinée au dépôt et à la diffusion de documents scientifiques de niveau recherche, publiés ou non, émanant des établissements d'enseignement et de recherche français ou étrangers, des laboratoires publics ou privés.



A record of eruption and intrusion at a fast spreading ridge axis: Axial summit trough of the East Pacific Rise at 9–10°N

S. Adam Soule

Geology and Geophysics Department, Woods Hole Oceanographic Institution, Woods Hole, Massachusetts 02543, USA (ssoule@whoi.edu)

Javier Escartín

Groupe de Geosciences Marines, Institut de Physique du Globe de Paris, Centre National de la Recherche Scientifique, F-75252 Paris, France

Daniel J. Fornari

Geology and Geophysics Department, Woods Hole Oceanographic Institution, Woods Hole, Massachusetts 02543, USA

[1] High-resolution side-scan sonar, near-bottom multibeam bathymetry, and deep-sea photo and bathymetry traverses are used to map the axial summit trough (AST) at the East Pacific Rise between 9 and 10°N. We define three ridge axis morphologic types: no AST, narrow AST, and wide AST, which characterize distinct ridge crest domains spanning tens of kilometers along strike. Near-bottom observations, modeling of deformation above intruding dikes, and comparisons to the geologic and geophysical structure of the ridge crest are used to develop a revised model of AST genesis and evolution. This model helps constrain the record of intrusive and extrusive magmatism and styles of lava deposition along the ridge crest at time scales from hundreds to tens of thousands of years. The grabens in the narrow-AST domain (9°43′–53′N) are consistent with deformation above the most recent (<10) diking events beneath the ridge crest. Frequent high-effusion rate extrusive volcanism in this domain (several eruptions every ~100 years) overprints near-axis deformation and maintains a consistent AST width. The most recent eruption at the ridge crest occurred in this area and did not significantly modify the physical characteristics of the AST. The grabens in the wide-AST domain (9°23′–43′N) originated with similar dimensions to the narrow AST. Spreading, driven primarily by the intrusion of shallow dikes within a narrow axial zone, causes the initial graben bounding faults to migrate away from the axis. Infrequent extrusive volcanism (several eruptions every ~1000 years) fills a portion of the subsidence that accumulates over time but does not significantly modify the width of the AST. Outside of these domains, lower-effusion rate constructional volcanism without efficient drain-back fills and erases the signature of the AST. The relative frequency of intrusive versus extrusive magmatic events controls the morphology of the ridge crest and appears to remain constant over millennial time scales within the domains we have identified; however, over longer time scales (~10–25 ka), domain-specific intrusive-to-extrusive ratios do not appear to be fixed in space, resulting in a fairly consistent volcanic accretion over the length scale of the second-order ridge segment between 9°N and 10°N.

Components: 13,116 words, 9 figures.

Keywords: mid-ocean ridge; submarine volcanism; diking; seafloor morphology; magmatism.

Index Terms: 3035 Marine Geology and Geophysics: Midocean ridge processes; 3075 Marine Geology and Geophysics: Submarine tectonics and volcanism; 3045 Marine Geology and Geophysics: Seafloor morphology, geology, and geophysics.



Received 1 December 2008; Revised 6 July 2009; Accepted 15 July 2009; Published 22 October 2009.

Soule, S. A., J. Escartín, and D. J. Fornari (2009), A record of eruption and intrusion at a fast spreading ridge axis: Axial summit trough of the East Pacific Rise at 9–10°N, *Geochem. Geophys. Geosyst.*, 10, Q10T07, doi:10.1029/2008GC002354.

Theme: Recent Volcanic Eruptions, Properties, and Behavior of the Fast Spreading East Pacific Rise at 8°–11°N

Guest Editors: S. M. Carbotte, R. Haymon, and W. Seyfried

1. Introduction

[2] The global mid-ocean ridge (MOR) axis is a dynamic environment where volcanic accretion and tectonic deformation shape the architecture of the oceanic crust [e.g., *Macdonald*, 1982; *Buck and Poliakov*, 1998; *Karson*, 2002; *Karson et al.*, 2002], and the permeability structure controlling ridge crest hydrothermal circulation [e.g., *Wilcock*, 1998; *Fisher and Becker*, 2000; *German et al.*, 2004]. The relative contributions of magmatic accretion and tectonic deformation involved in building the oceanic crust vary widely between ridges spreading at different rates [e.g., *Carbotte and Macdonald*, 1994; *Searle et al.*, 1998; *Escartín et al.*, 1999; *Bohnenstiehl and Kleinrock*, 2000; *Martinez et al.*, 2006; *White et al.*, 2008]. Large-scale structural characteristics of MOR crests show clear evidence of the integrated effects of these processes over the range of spreading rates from ultraslow to superfast [*Hooft and Detrick*, 1995; *Karson*, 1998; *Small*, 1998; *Carbotte et al.*, 2006]. Slow to intermediate spreading ridges commonly contain a wide axial valley, up to 15 km across, with relief on the bounding faults of ~200 to >1000 m that develop over tens of thousands of years. Fast spreading MORs, like the second-order segment of the East Pacific Rise (EPR) between 9 and 10°N, are characterized instead by a broad rise ~8 to 10 km wide [e.g., *Macdonald et al.*, 1984, 1992; *Scheirer and Macdonald*, 1993], and lack a rift valley. Here, a narrow, 40–300 m wide, 5–15 m deep trough is often present at the ridge axis and serves as the locus of most volcanic and hydrothermal activity along the ridge crest (Figure 1) [*Haymon et al.*, 1991; *Gregg et al.*, 1996; *Fornari et al.*, 1998, 2004]. Comparable troughs are common along many fast and intermediate spreading rate ridge crests [e.g., *Macdonald and Fox*, 1988; *Cormier et al.*, 2003; *Chadwick and Embley*, 1998; *White et al.*, 2000; *Hey et al.*, 2004]. Detailed mapping and analysis of MOR axial trough mor-

phology and structure provide a basis for interpreting the recent magmatic and tectonic history of the most active part of the ridge crest.

[3] The generation of an axial summit trough (AST) at fast and intermediate spreading rate ridges has been attributed to a variety of volcanic and tectonic processes. *Fornari et al.* [1998] proposed that a narrow axial summit collapse trough (<100 m) forms through the draining of ponded lava flows through tubes or back into eruptive fissures, and as a result this purely volcanic feature widens over time by coalescing of these collapse features. They further suggest that variations in the character of the AST are expressed as part of an evolutionary cycle where volcanic troughs evolve to tectonic troughs as magmatism wanes, and are eventually reset to a magmatic “state” by reinvigorated volcanic activity that buries existing structures. *Cormier et al.* [2003] applied this model to the AST along the southern EPR, interpreting portions of the ridge crest in waxing and waning stages of magmatic activity as reflected in morphologic character and relative ages of seafloor lavas within the AST. *Lagabriele and Cormier* [1999] and *Carbotte et al.* [2003] suggest that wide axial grabens (>500 m) may originate from deflation of the underlying melt sill in a process analogous to caldera formation on terrestrial volcanoes. *Chadwick and Embley* [1998] proposed that the AST is dominantly a tectonic feature originating from deformation over intruding dikes that, in places, has been overprinted by volcanism so that it may appear narrower than its true tectonic dimensions. They suggest that, although accumulated deformation may occur in some locations, grabens are commonly generated by a single magmatic intrusion so that their width and depth reflect the combined effects of bounding fault steepness, dike intrusion depth, and dike width. Collectively, these studies suggest a wide range of potential processes that may contribute to AST formation

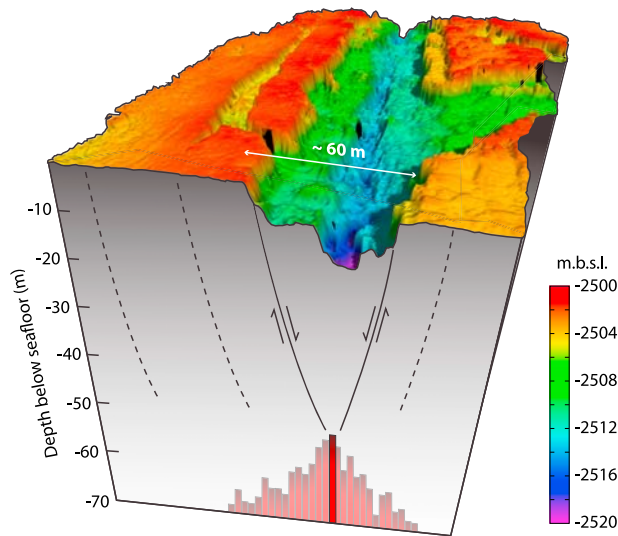


Figure 1. High-resolution seafloor bathymetry over the axial summit trough (AST) at $9^{\circ}50'N$ along the East Pacific Rise (EPR) looking roughly from north to south [Soule et al., 2008] with a color scale indicating depth in meters. The AST at this location is ~ 60 m wide and >10 m deep, including a central fissure from which the most recent lava flows erupted. A simplified model of the subsurface structure beneath the ridge crest, at 2X vertical exaggeration, shows the edges of the AST controlled by normal faults originating at the tip of an intruded but noneruptive dike. Older faults (dashed) may be present outboard of the current AST margins, but much of their relief has been filled by recent lava deposition.

and evolution, but further work is required to reconcile the various proposed models.

[4] This paper addresses the variability of processes responsible for AST formation and evolution along fast spreading ridges. We first describe the morphological character of the AST along ~ 100 km of the EPR crest interpreted from side-scan imagery, high-resolution microbathymetry, and digital seafloor imagery. In addition, we integrate recent interpretations of the volcanic and tectonic history of the EPR crest [e.g., Kurras et al., 2000; White et al., 2002; Fornari et al., 2004; Soule et al., 2005; Ferrini et al., 2007; Escartín et al., 2007] that provide the context for understanding the evolution of the AST. As the EPR in the area of $9^{\circ}50'N$ is the first MOR with multiple documented eruptions at the same location, we are also able to compare seafloor data collected before and after the 2005–2006 eruption of the EPR [Tolstoy et al., 2006; Cowen et al., 2007; Soule et al., 2007a], providing the first examination of how AST morphology is modified through a well-documented eruptive episode. All of these data are used to assess how

processes of faulting, volcanism, and diking are involved in the formation and evolution of the AST. Utilizing aspects of the models described above, we provide new constraints on the relative importance of tectonic deformation and volcanic overprinting in various stages of AST development and evaluate variability in magmatism and tectonism along the N. EPR ridge crest between $9^{\circ}N$ and $10^{\circ}N$ over time scales from hundreds to tens of thousands of years.

2. Data Description

[5] Over 6 years (2000, 2001, 2004 and 2006) we conducted field programs to the EPR between $9^{\circ}N$ and $10^{\circ}N$ using multiple near-bottom vehicle systems including a 120 kHz side-scan sonar (DSL-120a) [e.g., Scheirer et al., 2000; White et al., 2002], the autonomous vehicle ABE (Autonomous Benthic Explorer) [Yoerger et al., 1996], the submersible Alvin, and a deep-towed digital camera system (TowCam) [Fornari, 2003] (Figure 2). In addition to ship-based EM300 multibeam bathymetry [White et al., 2006], each near-bottom data set provides a unique perspective for characterizing the AST. The regional side-scan sonar provides areal dimensions of the AST and its relationship to adjacent volcanic and tectonic structures on the ridge crest. ABE bathymetry allows us to precisely measure AST depth and width at a local scale (2–4 km along axis). TowCam near-bottom profile data provide a high-resolution view of the AST dimensions constrained by seafloor imagery along across-axis profiles at numerous sites along the ridge crest (Figure 2b).

[6] Side-scan sonar backscatter imagery was collected with the DSL-120a system on two cruises: a regional $8 \text{ km} \times 80 \text{ km}$ area between $9^{\circ}25'N$ and $9^{\circ}55'N$ was imaged during a 2001 cruise (AT07-04) [Fornari et al., 2004] and a more AST-focused $2 \text{ km} \times 160 \text{ km}$ area between $9^{\circ}10'N$ and $10^{\circ}N$ was imaged during a 2000 cruise (Melville-AHANEMO2) [White et al., 2002] (Figure 2). Backscatter mosaics from both field programs are centered on the AST and provide detailed (2 m per pixel) imagery of seafloor acoustic texture that allow us to resolve individual faults, fissures, and volcanic features. These side-scan sonar data provide improved resolution and coverage relative to the Argo II 100 kHz data used to first describe the AST at the northern EPR (ASC in the works by Haymon et al. [1991, 1993] and Fornari et al. [1998]). High-resolution bathymetry was collected with ABE in 2000 (AT07-04) at ~ 40 m altitude using a 675 kHz scanning altimeter that provides a

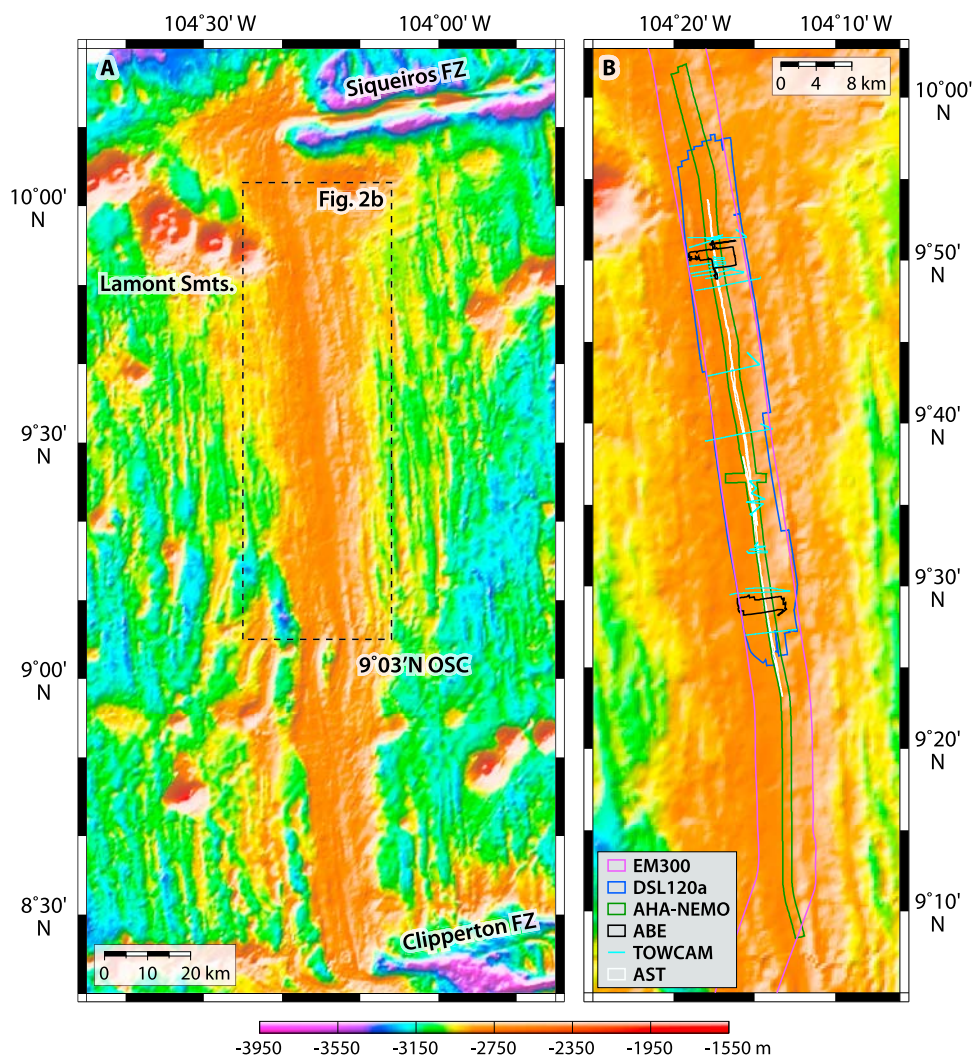


Figure 2. (a) Multibeam bathymetry [Macdonald *et al.*, 1992] shows the broad axial rise of the East Pacific Rise between the Clipperton and Siqueiros fracture zones. (b) The study area extends between 9°10'N and 10°00'N, within which side-scan sonar imagery was collected with the DSL120a on two cruises (AT7-4, blue; AHA-NEMO, green). EM300 multibeam bathymetry data (purple) covers the ridge crest through the study area [White *et al.*, 2006]. Two areas of high-resolution bathymetry were collected by scanning altimeter on ABE (black) at 9°50'N and 9°28'N. These data, along with numerous camera tows (cyan) collected across the ridge axis, were used to map the AST (white).

pixel resolution of 2 m × 5 m (horizontal) over two areas (~40 km² each) centered on the AST at 9°50'N and 9°30'N [Fornari *et al.*, 2004; Ferrini *et al.*, 2007]. Seafloor imagery and high-resolution (±10 cm) bathymetric profiles were collected with the WHOI TowCam during camera tows conducted in 2001 and 2004 (AT07-04, AT11-07). All the data are available through the Marine Geosciences Data System (MGDS, <http://www.marine-geo.org>).

[7] We have systematically picked the eastern and western limit of the AST from the DSL-120a side-scan sonar data at a spacing of ~50 m along the axis between 9°25'N to 9°55'N. The digital file of AST picks are available through the MGDS and

are provided in the auxiliary material to this paper.¹ The picks include the maximum possible across-axis extent of faults and fissures that define AST. As a check, we measured the AST dimensions from ABE bathymetry and TowCam profiles by identifying slope breaks associated with the trough walls. TowCam profile picks were correlated with the corresponding seafloor imagery by identifying extensive collapse or talus that marks the edge of the AST. We provide error bars on some TowCam estimates to reflect a maximum and minimum width, which either includes or excludes localized

¹Auxiliary materials are available in the HTML. doi:10.1029/2008GC002354.

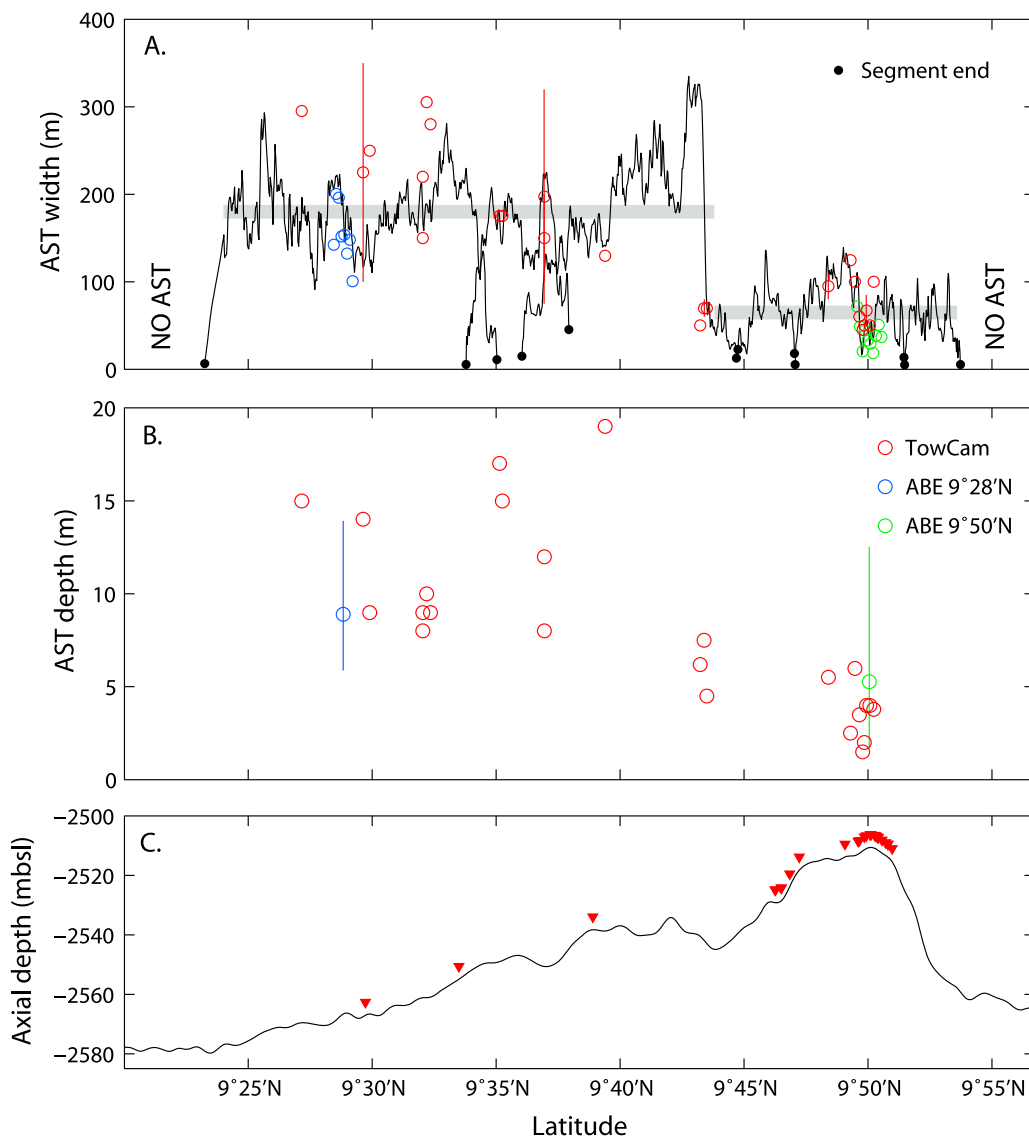


Figure 3. (a) The axial summit trough (AST) between 9°25'N and 9°58'N shows systematic variations in its width and depth. The width of the AST is measured from side-scan sonar imagery, and the mean width (gray bar) is ~100 m wider south of 9°43'N than it is to the north. Width estimates from TowCam and ABE bathymetry are in good agreement with estimates from side-scan sonar data. (b) The depth of the AST is measured from bathymetric profiles collected by TowCam and from high-resolution ABE bathymetry. AST depths from TowCam profiles within the wide AST domain are 2–15 m greater than in the narrow AST domain. AST depth can be highly variable over short distances as illustrated by the range of depths measured from ABE bathymetry (blue and green bars). (c) The transition from a wide to narrow AST is coincident with a decrease in axial depth (averaged over a 1 km wide corridor along the ridge crest from multibeam bathymetry [Macdonald *et al.*, 1992]) and an increase in the abundance of hydrothermal vents (inverted triangles). The transition to no AST north of 9°53'N is coincident with a marked increase in axial depth and an absence of hydrothermal vents. The transition to no AST south of 9°23'N shows a steady increase in axial depth and a similar absence of hydrothermal vents.

collapse features that commonly extend beyond what we would define as the AST [e.g., Engels *et al.*, 2003]. The overall width of the AST and its along-axis variations are consistent between all data sets (Figure 3a) and confirm that the side-scan records can be used for a regional interpretation of AST structure. We have used similar methods to map

the AST after the 2005–2006 eruption of the EPR [Tolstoy *et al.*, 2006; Cowen *et al.*, 2007; Soule *et al.*, 2007a] from posteruption DSL-120a side-scan sonar imagery and TowCam bathymetry profiles.

[8] The trace of the AST over the ~100-km-long area shows excellent correlation to detailed features



mapped in 1989 using an analog 100 kHz side-scan sonar [Haymon *et al.*, 1991; Fornari *et al.*, 1998]. The narrow across-axis perspective afforded by the 100 kHz swaths limited the interpretation of the AST at that time to identification of its presence or absence and rough dimensions along strike between 9°07'N and 9°55'N. Locally the trough position from 1989 is offset from the newly mapped position because of navigational discrepancies between the various data sets [e.g., Soule *et al.*, 2008], and to the analog mosaicing of the side-scan swaths. In comparison to the dimensions of the AST (referred to as ASCT by Fornari *et al.* [1998] and White *et al.* [2002]), which was described in a few locations from the 2000 survey [White *et al.*, 2002], we find that widths we measure in this study are similar, but that the AST is shallower by a factor of two than previous estimates. This discrepancy is likely due to the poorer vertical resolution of the DSL-120a phase shift bathymetry relative to the TowCam bathymetry profiles and ABE bathymetry used here.

[9] The extensive survey of AST and ridge crest terrain by the AT07-04 side-scan acquisition provides the most complete characterization to date of seafloor geology in this region. The overall geological interpretation of the sonar data shown in Figure 4 draws in part from previous mapping efforts [e.g., Soule *et al.*, 2005; Escartín *et al.*, 2007]. The AST, which runs along the peak of the ridge crest, is flanked by a 3–4 km wide band of highly reflective terrain that corresponds to recent (<10 ka) lava flows. Many lava flows contain channels that efficiently transport lava away from the axis [e.g., Auzende *et al.*, 1996; Sinton *et al.*, 2002; Soule *et al.*, 2005], allowing flows to either extend over older, moderately sedimented volcanic terrain, or dam against fault scarps or the flanks of volcanic pillow mounds [Macdonald *et al.*, 1989, 1996; Escartín *et al.*, 2007]. These pillow lava mounds are the primary expression of volcanic activity originating outside of the AST, and represent a small fraction of the total volcanic output along this section of the EPR [White *et al.*, 2002], the bulk of which is sourced from within the AST [Fornari *et al.*, 1998, 2004].

3. Characteristics of the AST

3.1. Ridge Crest Morphologic Domains

[10] We classify the ridge crest on the basis of the presence or absence of an AST and its physical dimensions as wide AST, narrow AST, and no AST

(Figure 5). This classification is similar to those of White *et al.* [2002]. In Figure 3 we show the along axis variations of AST width and depth as well as the overall axial depth. Despite variability in AST width (± 10 m) over short length scales that may be related to local mass-wasting of steep AST walls, the average width and depth are remarkably consistent over ridge crest morphologic domains that span tens of kilometers (Figure 3).

3.1.1. Wide AST

[11] Between 9°23'N and 9°43'N (~ 37 km), the ridge crest contains a 150–300 m wide graben of 8–20 m in depth (Figure 3b). In many locations the wide AST is defined by a series of inward facing faults that stair step and slightly rotate blocks within the graben [Fornari *et al.*, 1998; Cormier *et al.*, 2003; Escartín *et al.*, 2007] (Figure 5a). The floor of the wide AST contains broken lava crusts and areas of lightly sedimented, intact lobate and sheet flows. Between 9°37'N and 9°29'N, a narrow inner trough is present that is <50 m wide and ~ 3 –5 m deep. This feature is often associated with the most recent eruptive fissures [e.g., Cormier *et al.*, 2003; Fornari *et al.*, 2004], and active hydrothermal vents [Haymon *et al.*, 1991, 1993; Von Damm, 2000; Von Damm and Lilley, 2004].

3.1.2. Narrow AST

[12] Between 9°43'N and 9°52'N (~ 19 km), the ridge crest contains a 50–100 m wide graben with relief of 1–6 m (Figures 3b and 5b). The linearity and continuity of the AST margins along axis correspond to faults that define the narrow graben, although they may locally be modified by volcanic filling and subsequent collapse within the AST. The floor of the narrow AST contains broken lava crusts with lightly sedimented-to-unsedimented lobate and sheet flows as well as abundant lava pillars [e.g., Fornari *et al.*, 1998, 2004; Chadwick, 2003; Gregg and Chadwick, 1996; Gregg *et al.*, 2000]. We often are able to identify one or two fissures 1–10 m wide and ~ 5 m deep on the AST floor that are believed to represent the most recent eruptive fissures (Figure 1) [e.g., Ferrini *et al.*, 2007; Soule *et al.*, 2008]. High-temperature hydrothermal vents and associated sulfide vent structures are abundant within this ridge crest morphologic domain (Figure 3c), and are often found along the trace of the primary eruptive fissures [Haymon *et al.*, 1993; Wright *et al.*, 1995; Haymon and White, 2004; Fornari *et al.*, 2004].

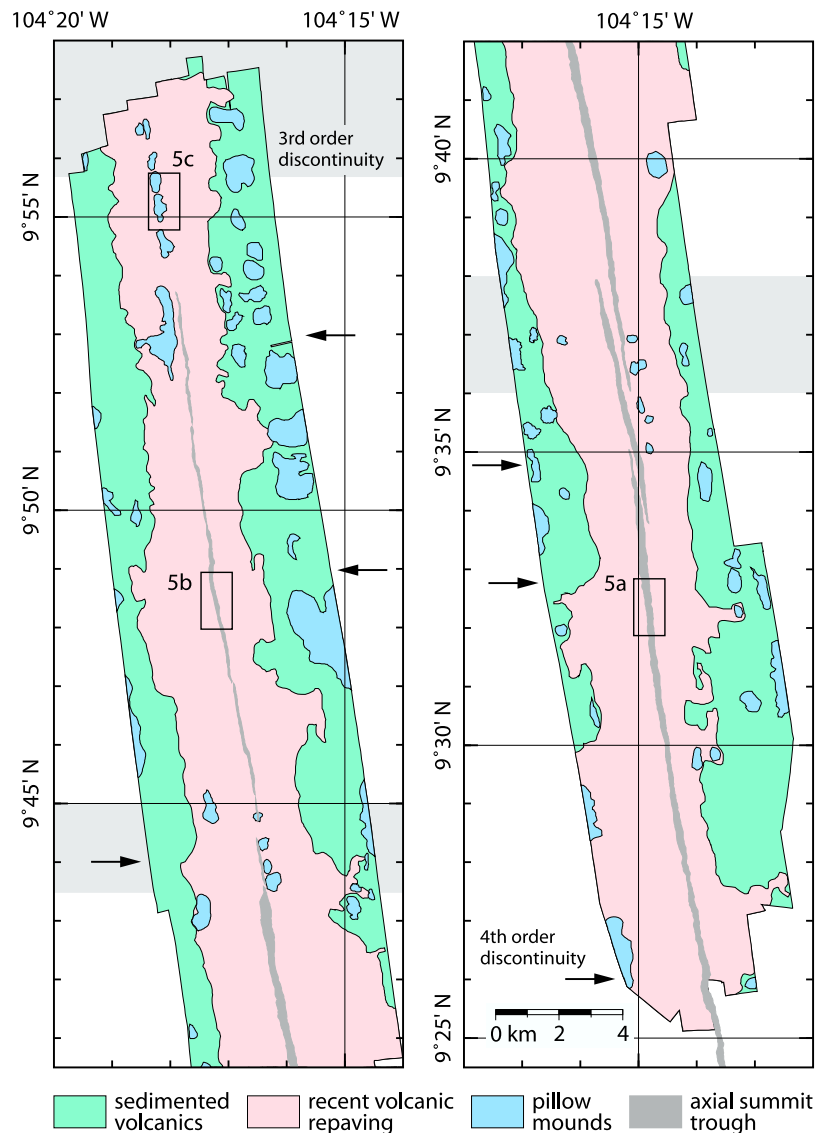


Figure 4. Simplified geological map of the East Pacific Rise crest between 9°25'N and 10°00'N. The extent of moderately sedimented, highly faulted volcanic seafloor (green) is limited to the outer edge of the DSL120a side-scan sonar data set collected on AT7-4. The zone of recent volcanic repaving (pink) is characterized by lightly sedimented lobate and sheet lava flows that extend 1.5 to >4 km from the ridge axis. Its boundaries, which are controlled in part by inward facing normal faults that dam flow advance, represent an age contrast of ~10 ka [Escartín *et al.*, 2007]. Numerous pillow mounds and ridges are present along the length of the ridge (blue), most commonly occurring outside recently repaved zone. Many pillow ridges appear to have erupted in situ [Sims *et al.*, 2003], up to 4 km from the ridge axis. The axial summit trough (AST) runs along the ridge axis and is composed of a number of segments separated by small-scale discontinuities. Boxes refer to type examples of these variable AST characteristics illustrated in Figure 5.

[13] The ridge crest in the narrow-AST domain is characterized by abundant lobate lava flows that emanate from the AST, drape the ridge crest, and are not cut by faults. The wide AST is characterized by similar lava flows, many of which are cut by inward facing faults. On the basis of our mapping, fault and fissure density (km/km^2) within a 500-m-wide corridor that encompasses the AST is 2–4 times greater within wide-AST domain than

the narrow-AST domain, indicating that tectonic deformation accumulated in recent times has not been as efficiently masked by volcanism in the wide AST domain [e.g., Escartín *et al.*, 2007].

3.1.3. No AST

[14] We find no discernable graben north of 9°53'N and south of 9°19'N. In each location, the ridge

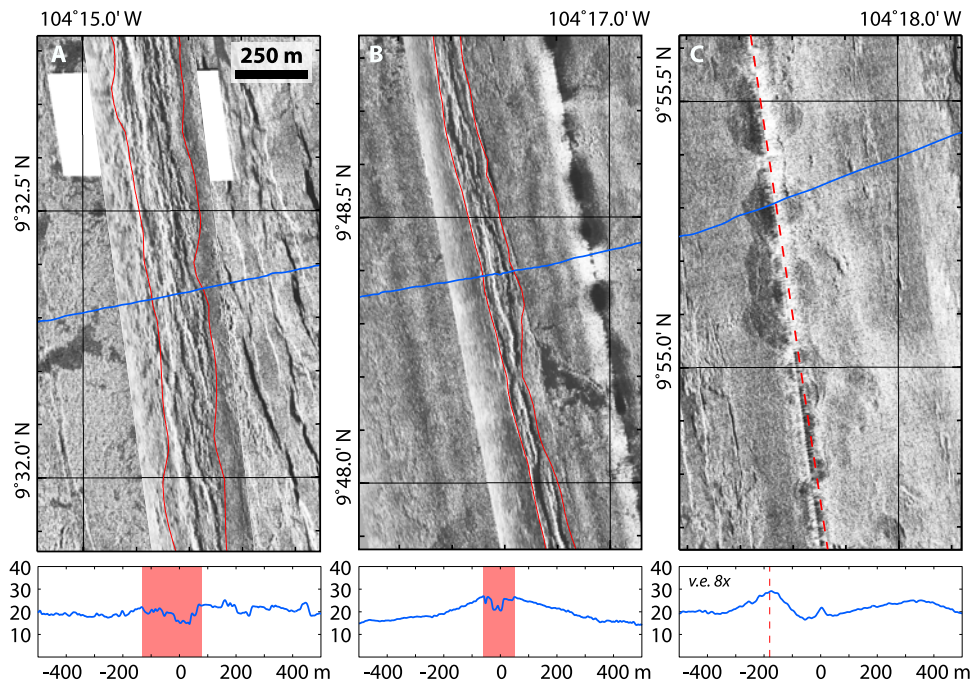


Figure 5. Examples of axial summit trough (AST) characteristics are shown in 120 kHz side-scan sonar backscatter imagery collected on the AHA-NEMO cruise and in ridge axis bathymetric profiles collected by TowCam. Bathymetry profiles have been filtered to remove high-frequency noise. (a) At 9°32'N, the AST is a ~200 m wide and ~10 m deep graben containing numerous fissures and faults which create a series of steps down to a narrow, inner graben. The ridge crest is relatively flat and has abundant signs of tectonic deformation indicating less frequent repaving by volcanic activity. (b) At 9°48.5'N, the AST is a well-defined, narrow graben ~100 m across and ~6 m deep. The ridge crest has a narrower axial high and is repaved by recent volcanism, including sheet flow-filled lava channels. (c) At 9°55'N, there is no discernable AST. Instead, the ridge axis is defined by a series of aligned volcanic mounds 100–200 m in diameter and 10–20 m high. The ridge crest here has a broad axial high, is smoothly paved by recent volcanism, and displays little tectonic deformation.

crest is characterized by an echelon fissures a few tens to hundreds of meters long and 5–20 m wide (Figure 5c) as well as small volcanic constructional features that are aligned roughly parallel to the ridge axis. North of 9°53'N the acoustic character of the ridge crest, outside of the fissure and pillow mound zone, is remarkably smooth volcanic seafloor lacking prominent flow front escarpments or lava channels [Kastens *et al.*, 1986; Haymon *et al.*, 1991], as are observed elsewhere in the study area. Between ~9°10'N and 9°23'N we have a limited perspective on the ridge crest with only a single swath of DSL-120a side-scan sonar data. No AST is resolved in the side-scan sonar or EM300 multi-beam bathymetry data [White *et al.*, 2006]. Some linear volcanic mounds are present along the ridge axis. The most distinctive features of the axial zone between 9°14–18'N are discontinuous collapse features and some lava channels suggesting widespread effusion and drain-back initiated collapse over the eruptive fissures.

3.2. Transitions and Continuity of AST Domains

[15] The EPR axial terrain between 9°12'N and 9°55'N is broken into seven third and four fourth-order segments on the basis of ridge axis morphology, hydrothermal vent distribution, relative age of lavas, and distribution of faulting and fissuring [Haymon *et al.*, 1991; Wright *et al.*, 1995; White *et al.*, 2002; Haymon and White, 2004; White *et al.*, 2006]. This fine-scale segmentation closely corresponds to our mapping of AST discontinuities (Figure 4) and domain transitions. The AST throughout the study area is made up of numerous segments that range in length from 4 to 20 km, with either breaks between AST segments or overlapping of AST segment ends. These segment ends are characterized by a narrowing and shallowing of the AST, which occurs over distances of ~100 m to ~1000 m for narrow and wide AST segments, respectively (Figure 3a). We note that the ridge

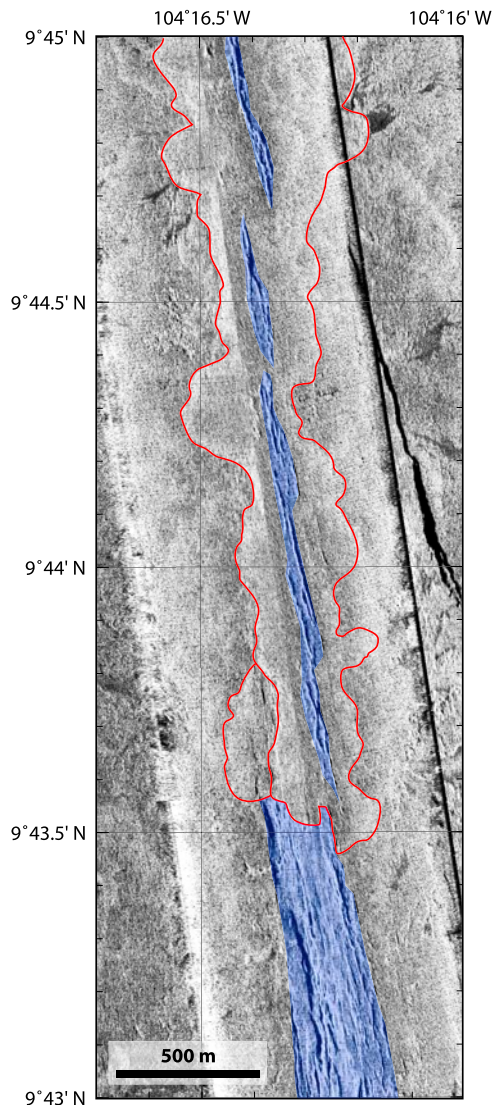


Figure 6. The transition between the wide-AST and narrow-AST domains at 9°43.5'N is shown in 120 kHz side-scan sonar backscatter imagery. The AST, shown in blue, is 200–300 m wide to the south of the transition and contains abundant faults and fissures. North of the transition, the AST is 50–100 m wide and is defined by a few fissures and faults. The most recent lava flows in the region are outlined in red. These flows have paved over axial deformation of the wide AST leaving a narrow trough over the zone of active dike intrusion.

crest domains defined above can include multiple third- and fourth-order segments, but that transitions occur at boundaries defined as third-order offsets.

[16] The transition from the narrow- to wide-AST domain occurs at ~9°43'N, and is characterized by a relay zone of discontinuous fissures previously identified as a third- or fourth-order axial discon-

tinuity [Haymon *et al.*, 1991; White *et al.*, 2002, 2006]. The side-scan sonar imagery shows that the wide, highly tectonized trough to the south is overprinted by recent volcanic activity to the north, filling and obscuring part of the wide-AST graben (Figure 6). The narrow, central portion of the graben remains open presumably because of efficient drain-back within the zone of active intrusion. AST depth is 4–8 m across this transition, spanning the lower limits of the wide AST and the upper limits of the narrow AST. The change in AST character from wide to narrow coincides with a shallowing of the ridge axis depth from 2560 ± 20 m south of 9°43'N to 2525 ± 15 m to the north (Figure 3c). In addition, it is located near the southernmost boundary of the most recent volcanic eruptions of the EPR ridge crest in 1991–1992 [Haymon *et al.*, 1993] and 2005–2006 [Soule *et al.*, 2007a].

4. AST Formation by Dike Intrusions

[17] Dike induced faults link high-tension zones found at the tip of a propagating dike and on the surface due to the horizontal displacements induced by the expanding, magma filled crack [e.g., Rubin and Pollard, 1988; Rubin, 1992; Pollard *et al.*, 1983; Mastin and Pollard, 1988]. This model has been widely applied to MORs [e.g., Chadwick and Embley, 1998; Curewitz and Karson, 1998; Wright, 1998; Carbotte *et al.*, 2006] and other rifted margins (e.g., Iceland, Afar) in order to explain the development of narrow grabens aligned with a rift axis. We use this model to examine the relationship between AST development and the geometry and frequency of intrusive versus extrusive magmatic events along the ridge crest.

[18] The geometry of normal faults related to dike intrusion is an actively debated topic. The most likely fault dip according to Mohr-Coulomb theory is ~60° [e.g., Jaeger and Cook, 1979]. However, observations in similar volcanic environments on land suggest dips that may be significantly higher. In Iceland, fault dips from 60° to 85° are observed [e.g., Gudmundsson, 1995; Angelier *et al.*, 1997]. In many cases, faults are nearly vertical at the land surface. These vertical scarps have been interpreted as shallow vertical fractures that form because of deformation induced by the slipping fault and link with more shallowly dipping faults at depth [Grant and Kattenhorn, 2004]. Vertical fractures related to normal faulting are also observed in Hawaii, although in that case the fractures are commonly

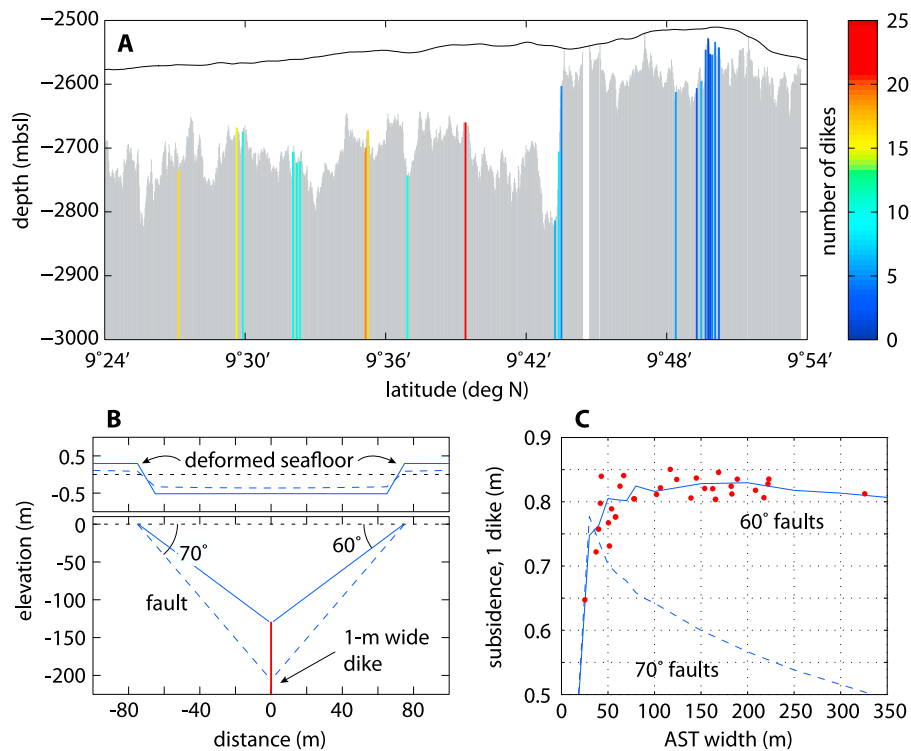


Figure 7. (a) The average depth of dikes intruding the ridge axis was calculated from (b) the width of the AST assuming that bounding faults at 60° originate at or near the tip of the intruding dike. We calculate the amount of subsidence associated with a 1-m-wide dike over a range of graben widths and for both 60° and 70° dipping faults. (c) With 60° faults, subsidence is roughly constant for graben widths >50 m both for a constant dike length of 1 km (blue line) and for varying dike lengths based on the observed depth to the AMC (red dots). With 70° faults, subsidence peaks at a graben width of <50 m and decreases with increasing graben width to a minimum that is ~0.6 times that for 60° faults. See section 4 for model parameters and description. The step change in width of the AST at 9°43'N (Figures 3a and 6) predicts a change in the mean dike depth from ~50 m (north) and ~150 m (south). We estimate the minimum number of dike intrusions necessary to subside the AST to its observed depth from a flat seafloor at locations where we have depth measurements at 2–8 where the AST is narrow and 10–25 where the AST is wide.

distinct from the fault surface [e.g., *Martel and Langley, 2006; Kaven and Martel, 2007*]. Others interpret near-vertical faults as reflective of the overall fault dip resulting from deflation of shallow sills, which would promote steeper dipping faults [e.g., *Tentler and Temperley, 2007*]. We have measured fault dips throughout our study area using high-resolution bathymetric profiles and find values ranging from 45° to 80°, with a mean of ~60°. Some of the variability in the dip angle we observe results from modification of fault scarps by lava flows and mass wasting, which tend to lower the observed dip, and from noise in high-resolution bathymetric data sets that may increase the maximum observed dip (see auxiliary material).

[19] For this work we assume a fault dip (α) of 60°–70°, a range that is consistent with measure-

ments from the study area, observations from similar environments, and theory. As a result, the graben width (w) would reflect the depth of the dike intrusion (d) with the following relationship, $w = 2[d \cdot \tan(\alpha)]$. On the basis of this simple geometrical relationship, we estimate a depth below the seafloor to the top of the intruding dikes, where the faults responsible for the AST (Figure 7a) originate. The mean (and 1 σ) dike intrusion depths in the narrow-AST domain are 56 (± 24) m to 89 (± 39) m and in the wide-AST domain are 156 (± 56) m to 250 (± 66) m. The lesser and greater depths within each domain reflect 60° and 70° dipping faults, respectively. This model, which assumes that the AST width is controlled exclusively by the depth of the intruding dikes, is useful for evaluating where (in the wide- or narrow-AST domain) this model is appropriate and where the



AST has been modified by volcanic overprinting or by accumulated tectonic deformation.

[20] We are able to use the dike intrusion depths inferred from AST width to model the vertical subsidence of the graben during a single dike intrusion and, by extrapolation, the minimum number of such events necessary to produce the observed relief across the graben in the places where we have well-constrained measurements. We use 3D-DEF, a three-dimensional boundary element model [Gomberg and Ellis, 1993], to simulate deformation on the graben bounding faults resulting from the intrusion of a 1-m-wide dike to a depth prescribed by the AST width. We define a 3D model space of $30 \times 30 \times 10$ km, much larger than the region of interest in order to eliminate edge effects. In the model we prescribe boundary conditions of no far-field stress and define faults dipping at 60° or 70° with a frictional coefficient of 0.6. We then impose dike opening of 1 m [e.g., Qin and Buck, 2008] on a vertical plane that extends from the estimated dike tip to a range of depths (Figure 7b) and examine the resulting surface deformation on a vertical plane at the center of the model space. All calculations were performed with a Young's modulus, E , of 30 GPa and a Poisson's ratio, ν , of 0.25 [Heap et al., 2009; Schultz, 1995].

[21] For dikes of a constant 1-km height, we find that subsidence ranges from 65 cm to 85 cm over the range of observed graben widths and for 60° faults. Graben widths >50 m all produce 80–85 cm of during a single 1-m-wide dike intrusion (Figure 7c). When dikes are allowed to extend to the depth of the AMC (~ 1.5 km) as measured by multichannel seismic profiles [Kent et al., 1993], we see only a slight variation in the amount of subsidence from the 1-km-tall dike results. When 70° faults are imposed, subsidence is smaller by up to a factor of 1.6 (Figure 7c) because of a greater depth to the dike tip and an unfavorable location of the faults relative to the surface deformation from dike opening (Figure 7b). From this analysis, we conclude that the AST, which in nearly all instances has relief in excess of 3 m, is not created during a single magmatic event. Instead, as suggested by Chadwick and Embley [1998], the trough depth is more likely a reflection of accumulated deformation from numerous dike intrusions reactivating existing faults. This model agrees with the interpretation that the EPR possesses a very narrow zone of repeated diking that has been inferred from the plan view distribution of lava flows emanating

from the AST (Figure 4) [Fornari et al., 2004; Soule et al., 2005].

5. Discussion

[22] The AST along the ~ 100 km of ridge crest examined in this study shows considerable complexity over short length scales (tens of meters) reflecting the stochastic nature of volcanism and tectonism at fast spreading MORs. However, over longer distances (kilometers), the AST possesses consistent physical characteristics that reflect the underlying processes that drive its development. On the basis of our observations of AST morphological and structural characteristics, modeling results, and our understanding of the geological and geophysical structure of the ridge crest and shallow crust, we suggest the following model for AST genesis and evolution, the details of which are described in sections 5.1–5.4.

[23] The AST, in all locations, reflects deformation that occurs above magmatic dikes that intrude to shallow crustal levels (~ 60 m) below the seafloor (bsf) within a very narrow (<100 m) zone along the ridge axis. Equivalent rates of dike intrusion to similar depths along the EPR axis result in similar amounts dike induced deformation and subsidence. Thus, irrespective of whether the AST is narrow or wide or absent, there is a common underlying structure that we suggest is modified by varying degrees of volcanic overprinting producing the range of characteristic AST morphologies. AST structure can be maintained through a major eruptive episode because of efficient drain-back within the central and most active portion of the AST, roughly coincident with the narrow zone of dike intrusion. However, we conclude that outside of the central portion of the AST, volcanic deposition effectively overprints near-axis deformation [Escartin et al., 2007]. As such, the narrow-AST domain displays deformation from only the most recent dike intrusions and its width better reflects the depth to which dikes intrude beneath the ridge crest. The wide-AST domain graben grows in width and depth, from an initial condition similar to that found in narrow AST segments, because of the continued emplacement of shallow dikes that cause the graben-bounding faults to migrate away from the narrow zone of intrusion while subsidence accumulates within the graben. Less frequent extrusive eruptions fill some of the wide-AST depth, but do not overprint the wider zone of deformation. Where no AST is observed, the graben has been filled either by eruptions that are particularly large,



or more commonly by low-effusion rate eruptions that produce constructional volcanic features such as pillow mounds that more effectively fill and pave over axial deformational features.

5.1. Narrow AST Genesis

[24] The change in AST width to the north and south $9^{\circ}43'N$ does not likely reflect a dike intrusion depth abruptly increasing from ~ 60 m to ~ 160 m bsf (Figure 7). Such a difference may be possible because of a decrease in magma chamber overpressure (i.e., pressure necessary to initiate diking relative to lithostatic pressure from overlying extrusive and intrusive rocks [Buck *et al.*, 1997]). Given the similarity in AMC reflector depth across the narrow-AST and wide-AST domains of ~ 1.5 km [Kent *et al.*, 1993], a change in overpressure would most likely arise because of a change in the density structure of the overlying column rocks [e.g., Cormier *et al.*, 2003]. However, seismic velocity structure, our best proxy of the shallow crustal density structure, does not differ significantly between the wide- and narrow-AST domains [e.g., Christeson *et al.*, 1992, 1996; Harding *et al.*, 1993; Sohn *et al.*, 2004] and are unlikely to result in a sizable change in average dike intrusion depths between the domains. Thus, we conclude that the inferred dike intrusion depths from AST width alone (Figure 7) are likely incorrect either for the wide-AST (too deep) or narrow-AST domain (too shallow).

[25] Chadwick and Embley [1998] suggest that dike induced graben formation is the most likely origin of the northern EPR AST. However, they note that the jagged edges, and talus covered floor of the AST at the northern EPR indicate that the true (i.e., tectonic) dimensions of the graben may become obscured by frequent volcanic eruptions that fill and drain it, accreting lava to both the trough sides and floor. This interpretation is comparable with that of Haymon *et al.* [1991], Fornari *et al.* [1998], and Cormier *et al.* [2003], who suggested that a narrow AST is likely a lava collapse feature formed by drain-back over eruptive vents. In general, the perception is that the narrower the AST, the more likely it is that its shape is controlled by volcanic rather than tectonic processes. On the basis of these interpretations, we might expect that narrow-AST domain widths are spuriously narrow because of volcanic overprinting.

[26] The recent 2005–2006 eruptions, which filled and overflowed the edges of the AST [Soule *et al.*,

2007a], provide insight into the effects of a volcanic eruption on AST morphology (Figure 8). Comparison of side-scan sonar data acquired before and after the eruptions indicate that the AST width is not significantly modified (mean difference of 1.8 m, Figure 8b). This is the case even though the trough was clearly filled and overflowed along most of the ~ 18 km of the ridge crest where the eruption occurred [Soule *et al.*, 2007a]. From TowCam profiles, we observe that the mean depth increases from ~ 4 m before to ~ 5 m after the eruption, although the data scatter is considerable in both surveys (Figure 8c). Possible causes of such an increase in AST depth are the increased height of the AST rims due to accretion of new lava, enhanced collapse of lava crusts on the AST floor, a tectonic subsidence that is greater than the infilling of the AST, or a combination of these processes. Overall, minor changes in AST morphology during the 2005–2006 eruptions indicate that volcanic overprinting within the most active portion of the AST is limited and does not necessarily cause the AST to become dramatically narrower or shallower. We conclude that drain-back of lava erupted in the AST, a critical component of the volcanic collapse model [Haymon *et al.*, 1991; Fornari *et al.*, 1998], is a key process for exposing the trough but that AST dimensions are dominantly controlled by dike induced faulting.

[27] Another test of the modeled dike intrusion depths comes from a comparison to the seismically imaged shallow crustal structure at the EPR crest, which can be indicative of the average dike intrusion depth beneath the ridge crest. The typical seismic velocity structure of the crust at fast and intermediate spreading rate ridges is characterized by an uppermost layer 2a, which comprises a seismic low-velocity layer (~ 2.33 m/s) underlain by a transitional zone (~ 2.5 – 5 m/s). On the basis of comparisons to observed structure in ophiolites, tectonic windows, and drill holes, the seismic low-velocity layer is believed to reflect extrusive lavas while the transition zone reflects a mixture of extrusive lavas and dikes. However, alternative interpretations such as layer of high porosity due to extensive cracking [e.g., Christeson *et al.*, 2007] have not been ruled out. Layer 2b (~ 5 m/s) underlies the transition zone and is thought to reflect a region composed entirely of sheeted dikes. For this study, we assume that the midpoint of the transition zone between layer 2a and 2b velocities is the best proxy of the time-averaged dike intrusion depth beneath the ridge crest.

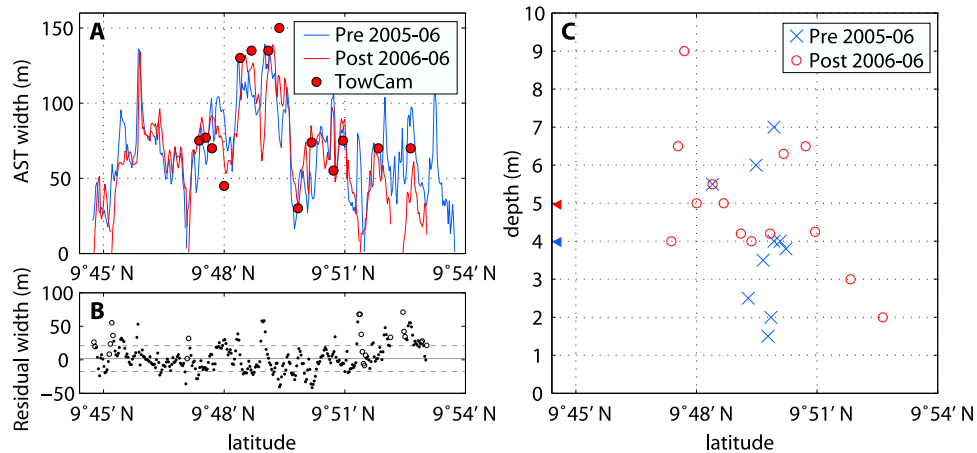


Figure 8. (a) The width of the axial summit trough (AST) after the 2005–2006 eruption of the EPR [Soule *et al.*, 2007a], mapped from side-scan sonar imagery [Soule *et al.*, 2007b], shows excellent agreement to the preeruption AST. The post 2005–2006 AST width agrees with point measurements from TowCam crossings collected after the eruption. (b) Residuals between the preeruption and posteruption AST width are randomly distributed about a mean of 1.8 m (solid line) with a standard deviation of 19 m. Locations where the measured AST width is less than 20 m (open circles), commonly found at the ends of AST segments, are not included in the analysis as they may have gone undetected in the preeruption AST mapping. Many of the largest differences in width can be attributed to areas where the side-scan nadir interfered with AST mapping preeruption or posteruption. The 2005–2006 lava was erupted from the AST between 9°46'N and 9°53'N [Soule *et al.*, 2007a]. (c) The depth of the AST preeruption and posteruption agrees well although AST depth was rarely measured in the same location. Although there is significant variability in the AST depth, mean depths within the eruption area, shown by left facing triangles, are similar at ~4 m preeruption and ~5 m posteruption.

[28] High-resolution seismic refraction studies conducted at 9°50'N (within the narrow-AST domain) [Sohn *et al.*, 2004] and 9°30'N (within the wide-AST domain) [Christeson *et al.*, 1992] reveal an axial seismic structure with transition zone depths of ~50 m and ~75 m, respectively. We recognize the limitations of such an estimate due to uncertainties in velocity models that can be larger than 50 m vertically [e.g., Nedimovic *et al.*, 2008] and spatial averaging that may occur within the region sampled by refracted waves. However, absent direct observation, these data represent the highest-resolution view of the ridge crest velocity structure available in this region. This seismic proxy for time-averaged dike intrusion depth is consistent with dike intrusion depths inferred from AST width for narrow-AST domain (56–89 m), and significantly shallower than those inferred for the wide-AST domain. Given the concordance with the geophysical structure of the EPR crest in the study area and the lack of AST modification by the recent eruptive events, we conclude that the dimensions of the narrow-AST grabens better reflect the typical dike intrusion depths and that the wide-AST grabens reflects the evolution of an axial graben with diminished volcanic deposition/repaving.

5.2. Evolution of the Wide AST

[29] We propose that the wide AST originates with similar dimensions to the narrow AST and subsequently widens and deepens. The character of the AST where it is wide, with down-stepping walls from rim to floor and the presence of a narrow inner trough (Figure 5a), along with a greater density of faulting and fissuring in wider AST areas [e.g., Wright *et al.*, 1995] (Figure 6), support this. Two models for graben widening have been proposed for fast and intermediate spreading MORs. Carbotte *et al.* [2006] suggest that grabens may grow by accumulated magmatic spreading, wherein intrusion of noneruptive dikes slowly push apart the graben bounding faults and induce subsidence. We refer to this as the steady magmatic model as it does not require any change in the underlying magmatic system. Alternatively, Cormier *et al.* [2003] suggest that grabens widen over time because of less frequent dike intrusions to greater depths beneath the ridge crest (i.e., shorter dikes). We refer to this as the waning magmatic model as it requires a relative decrease in time of the magmatic overpressure driving dike intrusions. We note that these models refer specifically to the underlying magmatic system and that the frequency and vol-



ume of extrusive volcanic eruptions may or may not differ between them.

[30] The preponderance of evidence in our study area is consistent with a steady magmatic model rather than a waning magmatic model. As stated above, we do not see evidence for a magmatic system in decline such as an increasing depth to the underlying melt lens [e.g., *Cormier et al.*, 2003]. In addition, the shallow crustal structure imaged using seismic refraction [*Sohn et al.*, 2004; *Christeson et al.*, 1996] indicates that dike intrusion depths are not significantly different between the wide and narrow AST domains. Both the wide and narrow AST domains contain lightly sedimented lava flows in the near-axis region [*Soule et al.*, 2005], however, many of the flows in the wide AST domain are cut by faults [*Escartín et al.*, 2007] suggesting greater eruption repose intervals than within narrow AST domain. We often observe a narrow inner trough along portions of the wide AST that is similar in width and depth to the narrow AST suggesting deformation related to recent dike emplacement to a depth comparable to that of the narrow AST domain.

[31] A primary difference between the steady and waning magmatic models is the number of diking events necessary to produce the wide AST. The waning magmatic model, where dikes intrude to greater depths beneath the ridge crest, requires only as many diking events as are necessary to produce the observed subsidence (10–25, Figure 7). Assuming that the wide AST initiated with similar dimensions to those of the narrow AST, the steady magmatic model requires at least 100 dikes (assuming an average dike width of 1 m [e.g., *Curewitz and Karson*, 1998; *Qin and Buck*, 2008]) so that the initial graben bounding faults are rafted off-axis to a distance ~ 50 m from their original position. On the basis of our modeling results, this number of dike intrusions would induce subsidence of 35–40 m, much greater than the AST depths of 8 m to 20 m that we observe within the wide-AST domain. Our observations indicate that wide portions of the AST are floored with lightly sedimented (i.e., relatively recent) lava flows. We believe a large fraction of the total subsidence accumulated in the wide-AST domain has been filled by infrequent volcanic eruptions with a recurrence interval of hundreds to a thousand years [e.g., *Perfit et al.*, 1994; *Cormier et al.*, 2003].

[32] The model described above conflicts with previously proposed models in which a wide

AST may form because of deflation of the axial melt lens [e.g., *Macdonald and Fox*, 1988; *Lagabriele and Cormier*, 1999]. In that model, melt extraction and/or compaction results in deformation in the overlying crust along steeply dipping or vertical faults analogous to caldera collapse. On the basis of our mechanical models, melt extraction from a 1.5 km deep melt lens would produce deformation over a much larger area (1–4 km) than that of the AST (<200 m). The collapse model is viable for very wide ASTs, 500–2000 m in width, but is not appropriate for the scale of AST observed on this portion of the EPR.

5.3. Time Scale of AST Development

[33] Our modeling produces two estimates of the approximate number of dike events represented by the AST: one based on depth, another on width. The depth-based estimates (waning magmatic model) suggest the narrow-AST domain has formed over <10 diking events and the wide-AST domain over 10–25 dike events. The width-based estimates (steady magmatic model), which require occasional eruptive events that infill some portion of the AST depth, suggest a similar number of dike events for the narrow AST, and >100 dike events for the wide AST. Assuming a recurrence interval of roughly one diking event every 10 years [e.g., *Hooft et al.*, 1996; *Curewitz and Karson*, 1998], the narrow AST would develop over less than 100 years with both models and the wide AST during either 200–300 years or >1000 years for the waning and steady magmatic models, respectively. These estimates may slightly overpredict the development time, as we do not include the tectonic strain that is not associated with dike intrusions, which may account for up to 10% of total plate separation [*Escartín et al.*, 2007].

5.4. Volcanic Overprinting

[34] As described above, volcanic overprinting or the lack thereof plays a significant role in controlling the observed dimensions of the AST. In the narrow AST domain volcanic overprinting occurs outside of the most active (and narrowest) portion of the AST where drain-back is inefficient because of the lack of primary eruptive fissures (Figure 6). In the wide AST domain, less frequent volcanic overprinting fills AST depth, but does not modify AST width. In both areas, the volcanic morphology of the ridge crests suggests that moderate- to high-effusion rate eruptions are most common [e.g., *Kurras et al.*, 2000]. In contrast, portions of



the ridge crest with “no AST” appear to have experienced the greatest degree of volcanic overprinting. Previous models of AST evolution have suggested that large or more frequent volcanic eruptions “reset” the ridge crest, erasing the surface expression of the AST and initiating a new magmatic-tectonic cycle [Macdonald and Fox, 1988; Fornari *et al.*, 1998]. The stability of the narrow-AST dimensions and character before and after the 2005–2006 eruptions (Figure 8), which were volumetrically large for this portion of the EPR [Soule *et al.*, 2007a], suggests that this is not always the case. In addition, other proxies for an elevated magmatic budget and high eruption frequency such as inflated ridge crest morphology [e.g., Macdonald *et al.*, 1992; Scheirer and Macdonald, 1993] and abundance of high temperature vents [e.g., Haymon *et al.*, 1991; Wright *et al.*, 1995; Haymon and White, 2004; Von Damm, 2000; Von Damm and Lilley, 2004] are not present along ridge sections that we identify as having no AST.

[35] We conclude that areas along the EPR axis that lack an AST are not necessarily the product of large or frequent volcanic events. Instead, we suggest that a change in the style of eruption from high-effusion rate eruptions that produce lobate and sheet flows (such as the 2005–2006 eruption) to low-effusion rate eruptions that produce constructional volcanic features with abundant pillow lava may be a dominant factor controlling the absence of an AST. Low-effusion rate eruptions are less likely to experience extensive or efficient drain-back after the eruption ceases, a process that appears to be critical for exposing the AST dimensions controlled by dike-induced deformation. Evidence for such behavior is apparent north of 9°53'N and south of 9°23'N, where the trace of the ridge crest is defined by aligned pillow mounds and fissures rather than a well-defined AST. Low-effusion rate eruptions are commonly observed at the ends of magmatically active ridge segments [e.g., White *et al.*, 2002, 2006] and would help explain the position of the no-AST domains along the EPR axis. This model may not explain all portions of the ridge crest without an AST. At 9°16'–18'N, the ridge crest has no AST, but also shows evidence for high-effusion rate eruptions (e.g., sheet flows and extensive collapse features). In addition, the axial melt lens in this region is thought to be significantly wider than elsewhere along the ridge crest [Kent *et al.*, 1993], which may not be conducive to lower eruption rates. Although we have a narrower perspective on the ridge crest

geology in this region because of limited side-scan sonar coverage, this region may be an example of how a large volume, high-eruption rate volcanic event may also fill and erase the AST.

5.5. Implications for Along-Axis Magmatic Processes

[36] We have investigated how variations in the physical characteristics of the AST reflect varying rates of volcanic extrusion versus magmatic intrusion over hundred- to thousand-year time scales. On the basis of our interpretations of AST morphology and structure, we suggest that the narrow-AST domain (9°43'N to 9°53'N) has experienced more frequent volcanic eruptions than the wide-AST domain (9°25'N to 9°43'N), but similar frequency and geometry of diking over a period of at least 1000 years. The domains we have identified are well correlated with the fine-scale segmentation of the ridge crest [e.g., Haymon and White, 2004; Wright *et al.*, 1995; White *et al.*, 2002, 2006]. All of the ridge crest morphologic domains that we have identified span multiple fourth-order ridge crest discontinuities. The boundaries between AST domains occur at or near previously identified third-order discontinuities. Fourth-order discontinuities are thought to reflect shallow crustal processes (e.g., diking and cracking) while third-order discontinuities are thought to reflect variations in the geometry and rate of melt supply to lower crustal and midcrustal levels [e.g., Macdonald *et al.*, 1991, 1992; Haymon, 1996; Haymon and White, 2004]. Our results support this conclusion as we interpret variations in AST properties to reflect variations in intrusive versus extrusive magmatic activity, a property of the magmatic system that is more likely to vary *between* magmatic segments than within them. However, we note that the wide-AST domain spans two third-order segments, indicating that adjacent segments need not have distinct magmatic systems or that there may be significant communication in crustal melt supply/storage between adjacent segments.

[37] The difference in AST dimensions between the narrow and wide domains suggest that over the last 1000 years, roughly eight times as much lava has been deposited in the narrow AST domain. Longer time scale indicators of volcanic deposition, however, do not show similar variations to those identified from AST characteristics. The integrated volume of seismic layer 2a [Harding *et al.*, 1993] out to 3 km from the ridge axis, which represents ~25,000 years of volcanic accretion,

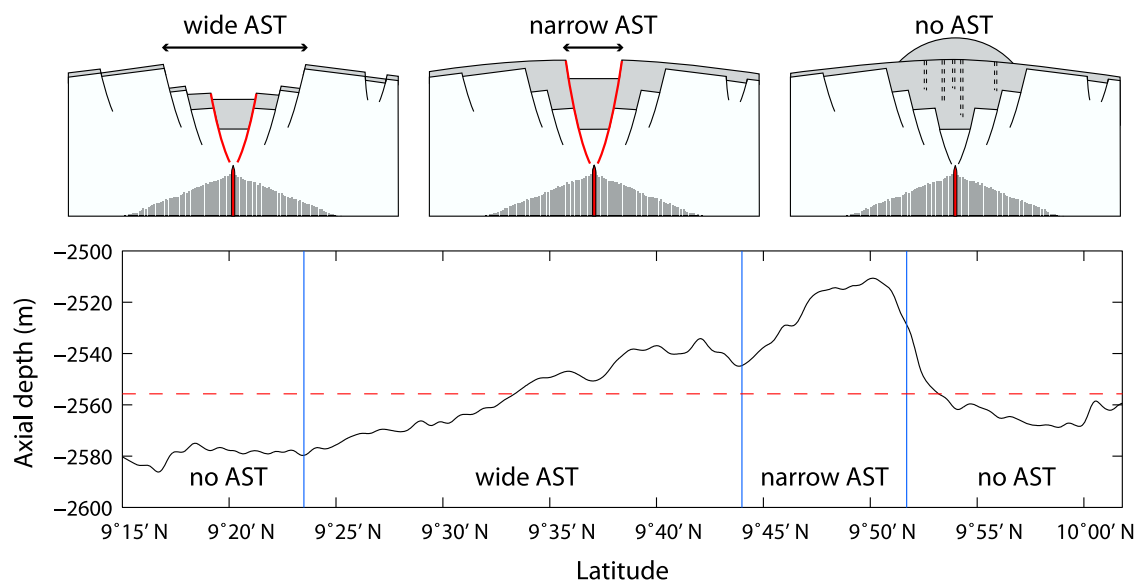


Figure 9. Schematic model of AST formation and evolution. The AST has an underlying structure (white) that is similar everywhere along the ridge crest and develops because of repeated diking to a consistent depth beneath the ridge crest. Those dikes are responsible for deformation on the innermost set of faults (red) and minor deformation on outboard faults. Varying levels of recent extrusive volcanic activity (gray) result in AST dimensions reflecting only the most recent diking events (e.g., <10, narrow AST) or a longer history of tectonic deformation (e.g., >100, wide AST). Elsewhere, lower-effusion rate constructional volcanism paves over the AST, through the emplacement of pillow mounds aligned with the ridge axis. In this case a greater proportion of the erupted material is deposited at the ridge axis rather than flowing across the ridge crest or back into the eruptive fissures. The varying rates and styles of extrusive activity are organized into domains that are tens of kilometers long along the ridge crest and broadly correlate with other parameters indicative of magmatic vigor such as ridge crest depth, abundance of hydrothermal vents, and mapped areas of recent volcanic eruptions.

varies by less than 10% between the narrow- and wide-AST domains. Similarly, the width of the zone recently repaved by lava flows, which represents $\sim 10,000$ years of volcanic accretion [Escartín *et al.*, 2007] is of a similar width between the different AST domains (Figure 4). This suggests that over ~ 10 – 25 ka time scales, the entirety of the ridge crest has experienced similar levels of extrusive volcanism. Thus, the current along-axis variations in extrusive versus intrusive magmatism and organization/state of the magmatic system that may be driving these variations must not be fixed in space (along axis) over long time scales.

6. Conclusions

[38] The ridge crest displays three primary morphologic types identified by the characteristic width and depth of axial grabens: narrow AST (~ 50 m wide, < 5 m deep), wide AST (~ 150 m wide, > 10 m deep), and no AST. Despite significant variability over short length scales, these AST domains display relatively constant morphology over tens of kilometers along axis. The narrow-

AST domain coincides with a region that is known to be volcanically active in the recent past, with documented eruptions occurring in 1991–1992 and 2005–2006. The highest concentration of high-temperature hydrothermal vents also occurs within this domain. The wide-AST domain occurs in a region with a high concentration of faults and fissures in the axial zone, suggesting a lower frequency of volcanic repaving. Regions without an AST do not necessarily correlate with extant indicators of an elevated magmatic budget, such as shoaling ridge crest depth and inflated cross section [e.g., Scheirer and Macdonald, 1993], but they commonly contain volcanic constructional features generated by low-extrusion rate eruptions.

[39] We find that dimensions of the narrow AST best reflect the time-averaged dike intrusion depth beneath the EPR crest of 50–75 m bsf and conclude that its dimensions are controlled by dike-induced deformation. This is in contrast to previous models that viewed the narrow AST to be solely a volcanic collapse feature or a volcanically overprinted graben with dimensions narrower than its true tectonic width. As similar dike intrusion



depths are observed from seismic refraction studies beneath both narrow- and wide-AST domains, we conclude that the wide AST evolved to its current state through magmatic spreading driven by shallowly intruded dikes within a narrow zone. The near-axis region of the wide-AST domain experiences less frequent volcanic repaving, but a sizable proportion of the accumulated subsidence within the graben may have been obscured by eruptions that partially filled the AST floor (Figure 9). Where we observe no AST, we suggest that axial deformation has been completely overprinted by volcanic accretion. This accretion may result from large, high-effusion rate eruptions, but we suggest that low-effusion rate eruptions, with greater lava deposition at the ridge axis, may be more effective at overprinting the AST. We have shown that the 2005–2006 eruption, a high-effusion rate eruption whose size was typical to large for the northern EPR, resulted in only minor changes to the dimensions of the narrow AST.

[40] Given the consistency of the underlying magmatic system at the northern EPR in terms of axial magma chamber depth and depth of dike intrusions beneath the ridge axis, the morphology of the AST provides information on the relative frequencies of intrusion and eruption and temporal/spatial variations in effusion rate along the ridge crest. This proposed model for AST formation and evolution should apply generally to fast spreading ridge crests that display consistent axial melt lenses in terms of depth and productivity. At the EPR 9–10°N, discontinuities in the AST both within and between AST domains are consistent with previous interpretations of ridge crest segmentation and possibly reflect similar discontinuities within the underlying magmatic system. Correlating new perspectives on the fine-scale segmentation of the N. EPR magmatic system [e.g., Carbotte *et al.*, 2008] with our model of AST development may provide information on the current state of the magmatic system as it relates to its potential for producing extrusive eruptions.

Acknowledgments

[41] We are grateful to the captain and crew of the R/V *Atlantis* and the staff of the National Deep Submergence Facility for assistance in collecting the data used in this study. The Ridge 2000 program was essential in coordinating the cruises. The chief scientists of the various cruises on which the data were collected are thanked for their hard work and generosity (K. Von Damm, E. Klein, H. Schouten, and M. Tivey). We appreciate discussions with M. Behn, H. Schouten, M. Tivey, and M. Perfit. Thoughtful reviews

by S. White, R. Buck, and R. Haymon helped improve the manuscript. This is IGP contribution 2543. This work was supported by NSF grants OCE-0525863 to D. Fornari and S. A. Soule; OCE-0732366 to S. A. Soule; and OCE-9819261 to H. Schouten, M. Tivey, and D. Fornari and by CNRS to J. Escartin.

References

- Angelier, J., F. Bergerat, O. Dauteuil, and T. Villemin (1997), Effective tension-shear relationships in extensional fissure swarms, axial rift zone of northeastern Iceland, *J. Volcanol. Geotherm. Res.*, *19*, 673–685.
- Auzende, J.-M., et al. (1996), Recent tectonic, magmatic, and hydrothermal activity on the East Pacific Rise between 17°S and 19°S: Submersible operations, *J. Geophys. Res.*, *101*, 17,995–18,010.
- Bohnstiehl, D., and M. C. Kleinrock (2000), Fissuring near the TAG active hydrothermal mound, 26°N on the Mid-Atlantic Ridge, *J. Volcanol. Geotherm. Res.*, *98*, 33–48, doi:10.1016/S0377-0273(99)00192-4.
- Buck, W. R., and A. N. B. Poliakov (1998), Abyssal hills formed by stretching oceanic lithosphere, *Nature*, *392*, 272–275, doi:10.1038/32636.
- Buck, W. R., S. M. Carbotte, and C. Z. Mutter (1997), Controls on extrusion at mid-ocean ridges, *Geology*, *25*, 935–938, doi:10.1130/0091-7613(1997)025<0935:COEAMO>2.3.CO;2.
- Carbotte, S. M., and K. C. Macdonald (1994), Comparison of seafloor tectonic fabric at intermediate, fast, and super fast spreading ridges: Influence of spreading rate, plate motions, and ridge segmentation on fault patterns, *J. Geophys. Res.*, *99*, 13,609–13,631, doi:10.1029/93JB02971.
- Carbotte, S. M., W. B. F. Ryan, W. Jin, M.-H. Cormier, E. Bergmanis, J. Sinton, and S. M. White (2003), Magmatic subsidence of the East Pacific Rise (EPR) at 18°14'S revealed through fault restoration of ridge crest bathymetry, *Geochem. Geophys. Geosyst.*, *4*(1), 1008, doi:10.1029/2002GC000337.
- Carbotte, S. M., R. S. Detrick, A. J. Harding, J. P. Canales, J. Babcock, G. M. Kent, E. Van Ark, M. Nedimovic, and J. B. Diebold (2006), Rift topography linked to magmatism at the intermediate spreading Juan de Fuca Ridge, *Geology*, *34*, 209–212, doi:10.1130/G21969.1.
- Carbotte, S. M., J. C. Mutter, J. P. Canales, M. R. Nedimovic, H. Carton, M. Xu, K. Newman, M. Marjanovic, O. Aghaei, and L. Stowe (2008), New observations of the magmatic segmentation of the East Pacific Rise from Siquieros to Cliperton from a multi-streamer reflection imaging study, *Eos Trans. AGU*, *89*(53), Fall Meet. Suppl., Abstract B21A-0320.
- Chadwick, W. W. (2003), Quantitative constraints on the growth of submarine lava pillars from a monitoring instrument that was caught in a lava flow, *J. Geophys. Res.*, *108*(B11), 2534, doi:10.1029/2003JB002422.
- Chadwick, W. W., and R. W. Embley (1998), Graben formation associated with recent dike intrusions and volcanic eruptions on the mid-ocean ridge, *J. Geophys. Res.*, *103*(9), 9807–9825.
- Christeson, G. L., G. M. Purdy, and G. J. Fryer (1992), Structure of young upper crust at the East Pacific Rise near 9°30'N, *Geophys. Res. Lett.*, *19*, 1045–1048, doi:10.1029/91GL00971.
- Christeson, G. L., G. M. Kent, G. M. Purdy, and R. S. Detrick (1996), Extrusive thickness variability at the East Pacific



- Rise, 9°–10°N: Constraints from seismic techniques, *J. Geophys. Res.*, *101*, 2859–2873, doi:10.1029/95JB03212.
- Christeson, G. L., K. D. McIntosh, and J. A. Karson (2007), Inconsistent correlation of seismic layer 2a and lava layer thickness in oceanic crust, *Nature*, *445*, 418–421, doi:10.1038/nature05517.
- Cormier, M. H., W. B. F. Ryan, A. K. Shah, W. Jin, A. M. Bradley, and D. R. Yoerger (2003), Waxing and waning volcanism along the East Pacific Rise on a millennium time scale, *Geology*, *31*, 633–636, doi:10.1130/0091-7613(2003)031<0633:WAWVAT>2.0.CO;2.
- Cowen, J. P., et al. (2007), Volcanic eruptions at the East Pacific Rise near 9°50'N, *Eos Trans. AGU*, *88*, 81–83, doi:10.1029/2007EO070001.
- Curewitz, D., and J. A. Karson (1998), Geological consequences of dike intrusion at mid-ocean ridge spreading centers, in *Faulting and Magmatism at Mid-Ocean Ridges*, *Geophys. Monogr. Ser.*, vol. 106, edited by R. Buck et al., pp. 117–136, AGU, Washington, D. C.
- Engels, J. L., M. H. Edwards, D. J. Fornari, M. R. Perfit, and J. R. Cann (2003), A new model for submarine volcanic collapse formation, *Geochem. Geophys. Geosyst.*, *4*(9), 1077, doi:10.1029/2002GC000483.
- Escartín, J., P. A. Cowie, R. C. Searle, S. Allerton, N. C. Mitchell, C. J. MacLeod, and A. P. Slootweg (1999), Quantifying tectonic strain and magmatic accretion at a slow spreading ridge segment, Mid-Atlantic Ridge, 29°N, *J. Geophys. Res.*, *104*, 10,421–10,437.
- Escartín, J., S. A. Soule, D. J. Fornari, M. A. Tivey, H. Schouten, and M. R. Perfit (2007), Interplay between faults and lava flows in construction of the upper oceanic crust: The East Pacific Rise crest 9°25'–9°58'N, *Geochem. Geophys. Geosyst.*, *8*, Q06005, doi:10.1029/2006GC001399.
- Ferrini, V. L., D. J. Fornari, T. M. Shank, J. C. Kinsey, M. A. Tivey, S. A. Soule, S. M. Carbotte, L. L. Whitcomb, D. Yoerger, and J. Howland (2007), Submeter bathymetric mapping of volcanic and hydrothermal features on the East Pacific Rise crest at 9°50'N, *Geochem. Geophys. Geosyst.*, *8*, Q01006, doi:10.1029/2006GC001333.
- Fisher, A. T., and K. Becker (2000), Channelized fluid flow in oceanic crust reconciles heat-flow and permeability data, *Nature*, *403*, 71–74, doi:10.1038/47463.
- Fornari, D. J. (2003), A new deep-sea towed digital camera and multi-rock coring system, *Eos Trans. AGU*, *84*, 69–76, doi:10.1029/2003EO080001.
- Fornari, D. J., M. H. Edwards, R. M. Haymon, M. R. Perfit, and T. K. P. Gregg (1998), Axial summit trough of the East Pacific Rise 9°–10°N: Geological characteristics and evolution of the axial zone on fast spreading mid-ocean ridges, *J. Geophys. Res.*, *103*, 9827–9855, doi:10.1029/98JB00028.
- Fornari, D. J., et al. (2004), Submarine lava flow emplacement at the East Pacific Rise 9°50'N: Implications for uppermost ocean crust stratigraphy and hydrothermal fluid circulation, in *Mid-Ocean Ridges: Hydrothermal Interactions Between the Lithosphere and Oceans*, *Geophys. Monogr. Ser.*, vol. 148, edited by C. R. German, J. Lin, and L. M. Parson, pp. 187–218, AGU, Washington, D. C.
- German, C. R., J. Lin, and L. M. Parson (Eds.) (2004), *Mid-Ocean Ridges: Hydrothermal Interactions Between the Lithosphere and Oceans*, *Geophys. Monogr. Ser.*, vol. 138, 318 pp., AGU, Washington, D. C.
- Gomberg, J., and M. Ellis (1993), 3D-DEF: A user's manual, *U.S. Geol. Surv. Open File Rep.*, 93-547, 22 pp.
- Grant, J. V., and S. A. Kattenhorn (2004), Evolution of vertical faults at an extensional plate boundary, southwest Iceland, *J. Struct. Geol.*, *26*, 537–557, doi:10.1016/j.jsg.2003.07.003.
- Gregg, T. K., and W. W. Chadwick (1996), Submarine lava flow inflation: A model for the formation of lava pillars, *Geology*, *24*, 981–984, doi:10.1130/0091-7613(1996)024<0981:SLFIAM>2.3.CO;2.
- Gregg, T. K. P., D. J. Fornari, M. R. Perfit, R. M. Haymon, and J. H. Fink (1996), Rapid emplacement of a mid-ocean ridge lava flow on the East Pacific Rise at 9°46'–51'N, *Earth Planet. Sci. Lett.*, *144*, E1–E7, doi:10.1016/S0012-821X(96)00179-3.
- Gregg, T. K. P., D. J. Fornari, M. R. Perfit, W. I. Ridley, and M. D. Kurz (2000), Using submarine lava pillars to record mid-ocean ridge eruption dynamics, *Earth Planet. Sci. Lett.*, *178*, 195–214, doi:10.1016/S0012-821X(00)00085-6.
- Gudmundsson, A. (1995), Infrastructure and mechanics of volcanic systems in Iceland, *J. Volcanol. Geotherm. Res.*, *64*, 1–22, doi:10.1016/0377-0273(95)92782-Q.
- Harding, A. J., G. M. Kent, and J. A. Orcutt (1993), A multi-channel seismic investigation of upper crustal structure at 9°N on the East Pacific Rise: Implications for crustal accretion, *J. Geophys. Res.*, *98*, 13,925–13,944.
- Haymon, R. M. (1996), The response of ridge-crest hydrothermal systems to segmented, episodic magma supply, in *Tectonic, Magmatic, Hydrothermal and Biological Segmentation of Mid-ocean Ridges*, *Geol. Soc. Spec. Publ.*, *118*, 157–168, doi:10.1144/GSL.SP.1996.118.01.09.
- Haymon, R. M., and S. M. White (2004), Fine-scale segmentation of volcanic/hydrothermal systems along fast-spreading ridge crests, *Earth Planet. Sci. Lett.*, *226*, 367–382, doi:10.1016/j.epsl.2004.08.002.
- Haymon, R. M., D. J. Fornari, M. H. Edwards, S. M. Carbotte, D. Wright, and K. C. Macdonald (1991), Hydrothermal vent distribution along the East Pacific Rise crest (9°9'–54'N) and its relationship to magmatic and tectonic processes on fast-spreading mid-ocean ridges, *Earth Planet. Sci. Lett.*, *104*, 513–534, doi:10.1016/0012-821X(91)90226-8.
- Haymon, R. M., et al. (1993), Volcanic eruption of the mid-ocean ridge along the East Pacific Rise crest at 9°45'–52'N: Direct submersible observations of seafloor phenomena associated with an eruption event in April, 1991, *Earth Planet. Sci. Lett.*, *119*, 85–101, doi:10.1016/0012-821X(93)90008-W.
- Heap, M. J., S. Vinciguerra, and P. G. Meredith (2009), The evolution of elastic moduli with increasing crack damage during cyclic stressing of a basalt from Mt. Etna Volcano, *Tectonophysics*, *471*, 153–160, doi:10.1016/j.tecto.2008.10.10.0004.
- Hey, R., et al. (2004), Tectonic/volcanic segmentation and controls on hydrothermal venting along Earth's fastest seafloor spreading system, EPR 27°–32°S, *Geochem. Geophys. Geosyst.*, *5*, Q12007, doi:10.1029/2004GC000764.
- Hooft, E. E., and R. S. Detrick (1995), Relationship between axial morphology, crustal thickness, and mantle temperatures along the Juan de Fuca and Gorda Ridges, *J. Geophys. Res.*, *100*, 22,499–22,508.
- Hooft, E. E., H. Schouten, and R. S. Detrick (1996), Constraining crustal emplacement processes from the variation in seismic layer 2A thickness at the East Pacific Rise, *Earth Planet. Sci. Lett.*, *142*, 289–309, doi:10.1016/0012-821X(96)00101-X.
- Jaeger, J. C., and N. G. W. Cook (1979), *Fundamentals of Rock Mechanics*, 3rd ed., 593 pp. Chapman and Hall, New York.
- Karson, J. A. (1998), Internal structure of oceanic lithosphere: A perspective from tectonic windows, in *Faulting and Magmatism at Mid-Ocean Ridges*, *Geophys. Monogr. Ser.*,



- vol. 106, edited by W. R. Buck et al., pp. 177–217, AGU, Washington, D. C.
- Karson, J. A. (2002), Geologic structure of the uppermost oceanic crust created at fast- to intermediate-rate spreading centers, *Annu. Rev. Earth Planet. Sci.*, *30*, 347–384, doi:10.1146/annurev.earth.30.091201.141132.
- Karson, J. A., et al. (2002), Structure of uppermost fast-spread oceanic crust exposed at the Hess Deep Rift: Implications for subaxial processes at the East Pacific Rise, *Geochem. Geophys. Geosyst.*, *3*(1), 1002, doi:10.1029/2001GC000155.
- Kastens, K. A., W. B. F. Ryan, and P. J. Fox (1986), Structural and volcanic expression of a fast slipping ridge-transform-ridge-plate boundary: Sea MARC I and photographic surveys at the Clipperton transform fault, *J. Geophys. Res.*, *91*, 3469–3488, doi:10.1029/JB091iB03p03469.
- Kaven, J. O., and S. J. Martel (2007), Growth of surface-breaching normal faults as a three-dimensional fracturing process, *J. Struct. Geol.*, *29*, 1463–1476, doi:10.1016/j.jsg.2007.05.007.
- Kent, G. M., A. J. Harding, and J. A. Orcutt (1993), Distribution of magma beneath the East Pacific Rise between the Clipperton transform and the 9°17'N deval from forward modeling of common depth point data, *J. Geophys. Res.*, *98*, 13,945–13,969.
- Kurras, G. J., D. J. Fornari, M. H. Edwards, M. R. Perfit, and M. C. Smith (2000), Volcanic morphology of the East Pacific Rise Crest 9°49'–52'N: Implications for volcanic emplacement processes at fast-spreading mid-ocean ridges, *Mar. Geophys. Res.*, *21*, 23–41, doi:10.1023/A:1004792202764.
- Lagabriele, Y., and M.-H. Cormier (1999), Formation of large summit troughs along the East Pacific Rise as collapse calderas: An evolutionary model, *J. Geophys. Res.*, *104*, 12,971–12,988.
- Macdonald, K. C. (1982), Mid-ocean ridges: Fine scale tectonic, volcanic and hydrothermal processes within the plate boundary zone, *Annu. Rev. Earth Planet. Sci.*, *10*, 155–190, doi:10.1146/annurev.earth.10.050182.001103.
- Macdonald, K. C., and P. J. Fox (1988), The axial summit graben and cross-sectional shape of the East Pacific Rise as indicators of axial magma chambers and recent volcanic eruptions, *Earth Planet. Sci. Lett.*, *88*, 119–131, doi:10.1016/0012-821X(88)90051-9.
- Macdonald, K. C., J.-C. Sempere, and P. J. Fox (1984), East Pacific Rise from Siqueiros to Orozco fracture zones: Along-strike continuity of axial neovolcanic zone and structure and evolution of overlapping spreading centers, *J. Geophys. Res.*, *89*, 6049–6069, doi:10.1029/JB089iB07p06049.
- Macdonald, K. C., R. Haymon, and A. Shor (1989), A 220 km² recently erupted lava field on the East Pacific Rise near lat 8°S, *Geology*, *17*, 212–216, doi:10.1130/0091-7613(1989)017<0212:AKRELF>2.3.CO;2.
- Macdonald, K. C., D. S. Scheirer, and S. M. Carbotte (1991), Mid-ocean ridges: Discontinuities, segments and giant cracks, *Science*, *253*, 986–994, doi:10.1126/science.253.5023.986.
- Macdonald, K. C., et al. (1992), The East Pacific Rise and its flanks 8–18°: History of segmentation, propagation and spreading direction based on SeaMARC II and SeaBeam studies, *Mar. Geophys. Res.*, *14*, 299–344, doi:10.1007/BF01203621.
- Macdonald, K. C., P. J. Fox, R. T. Alexander, R. Pockalny, and P. Gente (1996), Volcanic growth faults and the origin of Pacific abyssal hills, *Nature*, *380*, 125–129, doi:10.1038/380125a0.
- Martel, S. J., and J. Langley (2006), Propagation of normal faults to the surface in basalt, Koae fault system, Hawaii, *J. Struct. Geol.*, *28*, 2123–2143, doi:10.1016/j.jsg.2005.12.004.
- Martinez, F., F. Taylor, E. T. Baker, J. A. Resing, and S. L. Walker (2006), Opposing trends in crustal thickness and spreading rate along the back-arc Eastern Lau Spreading Center: Implications for controls on ridge morphology, faulting, and hydrothermal activity, *Earth Planet. Sci. Lett.*, *245*, 655–672, doi:10.1016/j.epsl.2006.03.049.
- Mastin, L. G., and D. D. Pollard (1988), Surface deformation and shallow dike intrusion processes at Inyo Craters, Long Valley, California, *J. Geophys. Res.*, *93*, 13,221–13,235.
- Nedimovic, M. R., S. M. Carbotte, J. B. Diebold, A. J. Harding, J. P. Canales, and G. M. Kent (2008), Upper crustal evolution across the Juan de Fuca ridge flanks, *Geochem. Geophys. Geosyst.*, *9*, Q09006, doi:10.1029/2008GC002085.
- Perfit, M. R., D. J. Fornari, M. C. Smith, and J. F. Bender (1994), Small scale spatial and temporal variations in mid-ocean ridge crest magmatic processes, *Geology*, *22*, 375–379, doi:10.1130/0091-7613(1994)022<0375:SSSATV>2.3.CO;2.
- Pollard, D. D., P. T. Delaney, W. A. Duffield, E. T. Endo, and A. T. Okamura (1983), Surface deformation in volcanic rift zones, *Tectonophysics*, *94*, 541–584, doi:10.1016/0040-1951(83)90034-3.
- Qin, R., and W. R. Buck (2008), Why meter-wide dikes at oceanic spreading centers?, *Earth Planet. Sci. Lett.*, *265*, 466–474, doi:10.1016/j.epsl.2007.10.044.
- Rubin, A. M. (1992), Dike-induced faulting and graben subsidence in volcanic rift zones, *J. Geophys. Res.*, *97*, 1839–1858, doi:10.1029/91JB02170.
- Rubin, A. M., and D. D. Pollard (1988), Dike-induced faulting in rift zones of Iceland and Afar, *Geology*, *16*, 413–417, doi:10.1130/0091-7613(1988)016<0413:DIFIRZ>2.3.CO;2.
- Scheirer, D. S., and K. C. Macdonald (1993), Variation in cross-sectional area of the axial ridge along the East Pacific Rise: Evidence for the magmatic budget of a fast-spreading center, *J. Geophys. Res.*, *98*, 7871–7885, doi:10.1029/93JB00015.
- Scheirer, D. S., D. J. Fornari, S. E. Humphris, and S. Lerner (2000), High-resolution seafloor mapping using the DSL-120 sonar system: Quantitative assessment of sidescan and phase-bathymetry data from the Lucky Strike segment of the mid-Atlantic ridge, *Mar. Geophys. Res.*, *21*, 121–142, doi:10.1023/A:1004701429848.
- Schultz, R. A. (1995), Limits on strength and deformation properties of jointed basaltic rock masses, *Rock Mech. Rock Eng.*, *28*, 1–15, doi:10.1007/BF01024770.
- Searle, R. C., P. A. Cowie, N. C. Mitchell, S. Allerton, C. J. MacLeod, J. Escartin, S. M. Russell, P. A. Slootweg, and T. Tanaka (1998), Fault structure and detailed evolution of a slow spreading ridge segment: The Mid-Atlantic Ridge at 29°N, *Earth Planet. Sci. Lett.*, *154*, 167–183, doi:10.1016/S0012-821X(97)00160-X.
- Sims, K. E., et al. (2003), Aberrant youth: Chemical and isotopic constraints on the origin of off-axis lavas from the East Pacific Rise, 9°–10°N, *Geochem. Geophys. Geosyst.*, *4*(10), 8621, doi:10.1029/2002GC000443.
- Sinton, J., E. Bergmanis, K. Rubin, R. Batiza, T. K. P. Gregg, K. Gronvold, K. C. Macdonald, and S. M. White (2002), Volcanic eruptions on mid-ocean ridges: New evidence from the superfast spreading East Pacific Rise, 17°–19°S, *J. Geophys. Res.*, *107*(B6), 2115, doi:10.1029/2000JB000090.
- Small, C. (1998), Global systematics of mid-ocean ridge morphology, in *Faulting and Magmatism at Mid-Ocean Ridges*, *Geophys. Monogr. Ser.*, vol. 106, edited by W. R. Buck et al., pp. 1–25, AGU, Washington, D. C.



- Sohn, R. A., S. C. Webb, and J. A. Hildebrand (2004), Fine-scale seismic structure of the shallow volcanic crust on the East Pacific Rise at 9°50'N, *J. Geophys. Res.*, *109*, B12104, doi:10.1029/2004JB003152.
- Soule, S. A., D. J. Fornari, M. R. Perfit, M. A. Tivey, W. I. Ridley, and H. Schouten (2005), Channelized lava flows at the East Pacific Rise crest 9°–10°N: The importance of off-axis lava transport in developing the architecture of young oceanic crust, *Geochem. Geophys. Geosyst.*, *6*, Q08005, doi:10.1029/2005GC000912.
- Soule, S. A., D. J. Fornari, M. R. Perfit, and K. Rubin (2007a), New insights into mid-ocean ridge volcanic processes from the 2005–2006 eruption of the East Pacific Rise, 9°46'N–9°56'N, *Geology*, *35*, 1079–1082, doi:10.1130/G23924A.1.
- Soule, S. A., S. M. White, D. J. Fornari, V. L. Ferrini, and M. A. Tivey (2007b), Comparison of pre- and post-eruption surveys of the 2005–2006 East Pacific Rise volcanic event: Implications for fast-spreading mid-ocean ridge eruption processes, *Eos Trans. AGU*, *88*(52), Fall Meet. Suppl., Abstract V21A-0383.
- Soule, S. A., V. L. Ferrini, J. C. Kinsey, D. J. Fornari, C. Sellers, S. M. White, K. Von Damm, and S. Carbotte (2008), Navigational infrastructure at the East Pacific Rise 9°50'N area following the 2005–2006 eruption: Seafloor benchmarks and near-bottom multibeam surveys, *Geochem. Geophys. Geosyst.*, *9*, Q11T04, doi:10.1029/2008GC002070.
- Tentler, T., and S. Temperley (2007), Magmatic fissures and their systems in Iceland: A tectonomagmatic model, *Tectonics*, *26*, TC5019, doi:10.1029/2006TC002037.
- Tolstoy, M., et al. (2006), A sea-floor spreading event captured by seismometers, *Science*, *314*, 1920–1922, doi:10.1126/science.1133950.
- Von Damm, K. (2000), Chemistry of hydrothermal vent fluids from 9°–10°N, East Pacific Rise: “Time zero,” the immediate post-eruptive period, *J. Geophys. Res.*, *105*, 11,203–11,222, doi:10.1029/1999JB900414.
- Von Damm, K. L., and M. D. Lilley (2004), Diffuse flow hydrothermal fluids from 9°50'N East Pacific Rise: Origin, evolution and biogeochemical controls, in *The Subseafloor Biosphere at Mid-Ocean Ridges*, *Geophys. Monogr. Ser.*, vol. 144, edited by W. S. D. Wilcock et al., pp. 245–268, AGU, Washington, D. C.
- White, S. M., K. C. Macdonald, and R. M. Haymon (2000), Basaltic lava domes, lava lakes, and volcanic segmentation on the southern East Pacific Rise, *J. Geophys. Res.*, *105*, 23,519–23,536, doi:10.1029/2000JB900248.
- White, S. M., R. M. Haymon, D. J. Fornari, M. R. Perfit, and K. C. Macdonald (2002), Correlation between volcanic and tectonic segmentation of fast-spreading ridges: Evidence from volcanic structures and lava flow morphology on the East Pacific Rise at 9°–10°N, *J. Geophys. Res.*, *107*(B8), 2173, doi:10.1029/2001JB000571.
- White, S. M., R. M. Haymon, and S. Carbotte (2006), A new view of ridge segmentation and near-axis volcanism at the East Pacific Rise, 8°–12°N, from EM300 multibeam bathymetry, *Geochem. Geophys. Geosyst.*, *7*, Q12O05, doi:10.1029/2006GC001407.
- White, S. M., J. D. Meyer, R. M. Haymon, K. C. Macdonald, E. T. Baker, and J. A. Resing (2008), High-resolution surveys along the hot spot-affected Galápagos Spreading Center: 2. Influence of magma supply on volcanic morphology, *Geochem. Geophys. Geosyst.*, *9*, Q09004, doi:10.1029/2008GC002036.
- Wilcock, W. S. D. (1998), Cellular convection models of mid-ocean ridge hydrothermal circulation and the temperatures of black smoker fluids, *J. Geophys. Res.*, *103*, 2585–2596, doi:10.1029/97JB03252.
- Wright, D. (1998), Formation and development of fissures at the East Pacific Rise, implications for faulting and magmatism at mid-ocean ridges, in *Faulting and Magmatism at Mid-Ocean Ridges*, *Geophys. Monogr. Ser.*, vol. 106, edited by W. R. Buck, J. A. Karson, and Y. Lagabriele, pp. 137–151, AGU, Washington, D. C.
- Wright, D. J., R. M. Haymon, and D. J. Fornari (1995), Crustal fissuring and its relationship to magmatic and hydrothermal processes on the East Pacific Rise crest (9°12' to 54'N), *J. Geophys. Res.*, *100*, 6097–6120, doi:10.1029/94JB02876.
- Yoerger, D., A. Bradley, R. Bachmayer, R. Catanach, A. Duester, S. Liberatore, H. Singh, B. Walden, and M. A. Tivey (1996), Near-bottom magnetic surveys of the Coaxial Ridge segment using the Autonomous Benthic Explorer survey vehicle, *Ridge2000 Events*, *7*, 5–9.